Developmental Cell
Article

Exit from Proliferation during Leaf Development in *Arabidopsis thaliana*: A Not-So-Gradual Process

Megan Andriankaja,[1,2,4] Stijn Dhondt,[1,2,4] Stefanie De Bodt,[1,2,4] Hannes Vanhaeren,[1,2] Frederik Coppens,[1,2] Liesbeth De Milde,[1,2] Per Mühlenbock,[1,2] Aleksandra Skirycz,[1,2] Nathalie Gonzalez,[1,2] Gerrit T.S. Beemster,[1,2,3] and Dirk Inzé[1,2,*]

[1]Department of Plant Systems Biology, VIB, 9052 Gent, Belgium
[2]Department of Plant Biotechnology and Bioinformatics, Ghent University, 9052 Gent, Belgium
[3]Department of Biology, University of Antwerp, 2020 Antwerp, Belgium
[4]These authors contributed equally to this work
*Correspondence: dirk.inze@psb.vib-ugent.be
DOI 10.1016/j.devcel.2011.11.011

SUMMARY

Early leaf growth is sustained by cell proliferation and subsequent cell expansion that initiates at the leaf tip and proceeds in a basipetal direction. Using detailed kinematic and gene expression studies to map these stages during early development of the third leaf of *Arabidopsis thaliana*, we showed that the cell-cycle arrest front did not progress gradually down the leaf, but rather was established and abolished abruptly. Interestingly, leaf greening and stomatal patterning followed a similar basipetal pattern, but proliferative pavement cell and formative meristemoid divisions were uncoordinated in respect to onset and persistence. Genes differentially expressed during the transition from cell proliferation to expansion were enriched in genes involved in cell cycle, photosynthesis, and chloroplast retrograde signaling. Proliferating primordia treated with norflurazon, a chemical inhibitor of retrograde signaling, showed inhibited onset of cell expansion. Hence, differentiation of the photosynthetic machinery is important for regulating the exit from proliferation.

INTRODUCTION

The plant leaf, by providing the basis for energy capture, is at the core of plant growth and ultimately an important part of human economic activities. Leaf development is extremely plastic and leaf size depends on genetic predisposition, leaf position, and environmental conditions. Many specific aspects of leaf development have been studied in the model plant *Arabidopsis thaliana*, including leaf initiation (Barbier de Reuille et al., 2006), abaxial/adaxial differentiation (Braybrook and Kuhlemeier, 2010), vascular development (Scarpella et al., 2010), stomatal development (Peterson et al., 2010), cell-cycle regulation (Donnelly et al., 1999; Beemster et al., 2005; Boudolf et al., 2009), and trichome formation (Pesch and Hülskamp, 2009). Extensive collections of mutants in leaf shape and size have been generated (Berná et al., 1999; Horiguchi et al., 2006), but the regulatory networks that control growth and final organ size are still poorly understood (Byrne, 2005; Gonzalez et al., 2009). The development of a growing dicotyledonous leaf has been divided into three main stages: primordium initiation, primary morphogenesis, and secondary morphogenesis (Donnelly et al., 1999). Leaf primordia initiate off the flanks of the shoot apical meristem at regions of high auxin and low cytokinin accumulation (Traas and Monéger, 2010). During primary morphogenesis, leaf growth is sustained by successive cell divisions and specific structures, such as trichomes, vasculature, and stomata, begin to form. Lastly, during secondary morphogenesis, the cells cease proliferating and begin to expand, mainly by cell wall loosening that continues to fuel further leaf growth (Cosgrove, 2005). Thus, the overall change in cell size in a growing organ over time depends on the balance between cell growth and division rates (Green, 1976). As dividing cells also grow, we use the terms "proliferation" to refer to this joint activity (Beemster and Baskin, 1998) and "expansion" to cell growth without cell division.

The transition from cell proliferation to expansion is a complex process with many factors interacting to create a network of growth control at both the transcript and protein levels (Gonzalez et al., 2009). Over time, the transition was shown to proceed in a gradient down the leaf, with cell proliferation first ceasing in the tip and then progressively down the longitudinal axis (Donnelly et al., 1999; Kazama et al., 2010). Differences in the timing of this transition will affect the number of cells formed and therefore potentially also leaf size. To date, numerous leaf size mutants have been described (Lee et al., 2006; Gonzalez et al., 2009; Horiguchi et al., 2009; Pérez-Pérez et al., 2009). Some genes have been found also that alter leaf size by affecting the transition from primary to secondary morphogenesis, such as *SHORT-ROOT*, *DA1*, and *AINTEGUMENTA* (Mizukami and Fischer, 2000; Li et al., 2008; Horiguchi et al., 2009; Dhondt et al., 2010) and *KLUH/CYP78A5* and *GRF5* have been proposed to play a role in the arrest front progression (Gonzalez et al., 2010; Kazama et al., 2010). Curiously, inhibition of cell proliferation is often compensated by an induction in cell expansion, so that the effects on the whole organ size are often strongly diminished (De Veylder et al., 2001; Tsukaya, 2002, 2003; Beemster et al., 2003).

Transcriptome analysis of leaves at proliferation and expansion stages has allowed for the identification of many genes specific for proliferation and expansion (Beemster et al., 2005),

whereas other transcriptome studies have identified marker genes that can be used as predictors of the differentiation status of leaves (Efroni et al., 2008). Although these studies have contributed to the broad understanding of leaf and rosette development, many questions remain regarding which transcriptional events occur precisely during the crucial transition from primary to secondary morphogenesis. These transcriptional events are of prime interest because they could potentially regulate the final cell number and, thus, the overall leaf size.

Here, we characterized the progression of the third leaf of *Arabidopsis* through the transition from primary to secondary morphogenesis by using our image analysis algorithms to visualize and quantify the size and shape of the cells and transcriptome analysis to show that the transition from cell proliferation to expansion occurs abruptly and simultaneously with the onset of photomorphogenesis. We provide evidence that retrograde signaling from chloroplasts can affect the onset of transition from proliferation to expansion, revealing a previously unknown level of regulatory complexity during the transition from primary to secondary morphogenesis.

RESULTS

Image Analysis as a Tool to Quantify Positional Changes in Cell Morphology

In theory, the timing of the transition between primary and secondary morphogenesis determines the number of cells and, thus, to some extent, the final leaf size. This transition occurs when a significant increase in cell size is observed (Donnelly et al., 1999; Tsukaya, 2002; Beemster et al., 2003, 2005) and when the cell morphology changes from circular for proliferating cells to the typical jigsaw puzzle-shape for expanding and mature pavement cells. To map these morphological changes, third leaves of in vitro grown *Arabidopsis* seedlings were harvested daily from day 8 to 14 after stratification, which spans the transition from primary to secondary leaf morphogenesis. At these time points, the length of the leaves increased throughout the time series from 0.29 ± 0.01 mm (SEM) to 1.92 ± 0.12 mm (SEM) (data not shown). Representative leaves from each time point were used to microscopically draw the cells of the abaxial epidermis along the complete proximal-distal axis. As individual drawings contained up to 7,000 cells, we developed specific image-analysis algorithms to quantify and visualize the morphological and positional information of each cell (Figure 1). For this data extraction, guard cells and extremely large pavement cells lining the leaf margins and overlaying the midvein (see Figure S1 available online) were excluded from the drawings, because their size and shape were not representative for the developmental stage of the leaf. Pavement cell shape was measured with a circularity score ranging from 1 to 0, with 1 indicating a perfect circle. As the value approached 0, cells were progressively more lobed, indicative of expanding cells. Cell area, cell circularity, and the position of the center of mass of the pavement cells relative to the leaf tip were recorded. Cell shape and size gradients along the leaf lengths were visualized by coloring cells according to parameter values (Figures 1E and 1F). These in-house developed image-analysis algorithms allowed us to clearly visualize (Figures 1E and 1F) and quantify the changes in cell morphology along the length of transitioning leaves.

Pavement Cell Size and Shape: Indicators of the Developmental Stage during Early Leaf Development

At early time points (days 8 and 9), the cells maintained a high circularity and a low and relatively constant average cell area (approximately 100 μm^2 across the entire leaf length), a consequence of balanced cell division and cell growth rates and indicative of cell proliferation. At the start of day 10, cells in the leaf tip became larger and less circular, indicative of cell expansion (Figure 2), whereas at days 13 and 14, the cells at the leaf base also showed increased cell areas and reduced circularity scores, implying that the cells started to expand at all positions along the leaf length (Figure 2). Thus, at days 8 and 9, the third leaf consisted entirely of proliferating cells, whereas at day 10, the cells in the leaf tip started to expand and those at the base continued to proliferate. This gradient of cell proliferation and expansion persisted through days 11 and 12. At days 13 and 14, the majority of cells at the leaf base also began to expand. Interestingly, the trends of both changes in cellular shape and area were similar across the leaf length (Figures 2A and 2B). Between days 9 and 10, when the transition to cell expansion began at the tip, the cells differed significantly in both shape and area. As the pavement cell area increased in expanding cells, so too did the lobing of the cell (Figure S2). Thus, image analysis revealed that size and shape of pavement cells are correlated indicators of the developmental stage of the leaf.

The Cell Proliferation Gradient of Pavement Cells Is Established Rapidly and Then Abruptly Disappears

To characterize how the cell-cycle arrest front migrates along the leaf, we used cell area and circularity as parameters to delimit the proliferation and expansion zones in the leaf. As leaf 3 at days 8 and 9 consisted completely of proliferating cells, it was possible to use these two time points to establish size and shape thresholds to define proliferating cells. With a confidence interval of 99%, the criteria for proliferation were a circularity score greater than 0.3894 and a cell area smaller than 261.38 μm^2 (Figure 3A). These thresholds were applied to the later time points to determine which cells fit the shape and size criteria for proliferation (Figure S3). Subsequently, we performed image analysis to visualize these cells and to extract positional information (Figure 3B). The proliferation zone was defined as the region of the leaf where at least 90% of the cells in a bin met the proliferation criteria defined above (Figure 3B). At days 8 and 9, proliferating cells occurred at every position along the leaf, whereas, at days 13 and 14, nowhere could leaves qualify as proliferative anymore. From these analyses, we observed that the proliferation zone of the leaf comprised 63%, 53%, and 38% of the proximal-distal leaf axis at days 10, 11, and 12, respectively (Figure 3B). These findings were confirmed by profiling a CYCB1;1-D-box:GUS-GFP translational fusion (Figure S4A). The B-type cyclin gene *CYCB1;1* was expressed uniformly throughout all cell layers, further supporting the use of the epidermis as a marker for tracking cell proliferation in the leaf (Figure S4B). Thus, between days 9 and 10, the proliferation zone was rapidly delimited; from days 10 to 12, it gradually decreased across the proximal-distal axis throughout transition; and between days 12 and 13, it was rapidly consumed because no zones had more than 90% proliferative cells anymore.

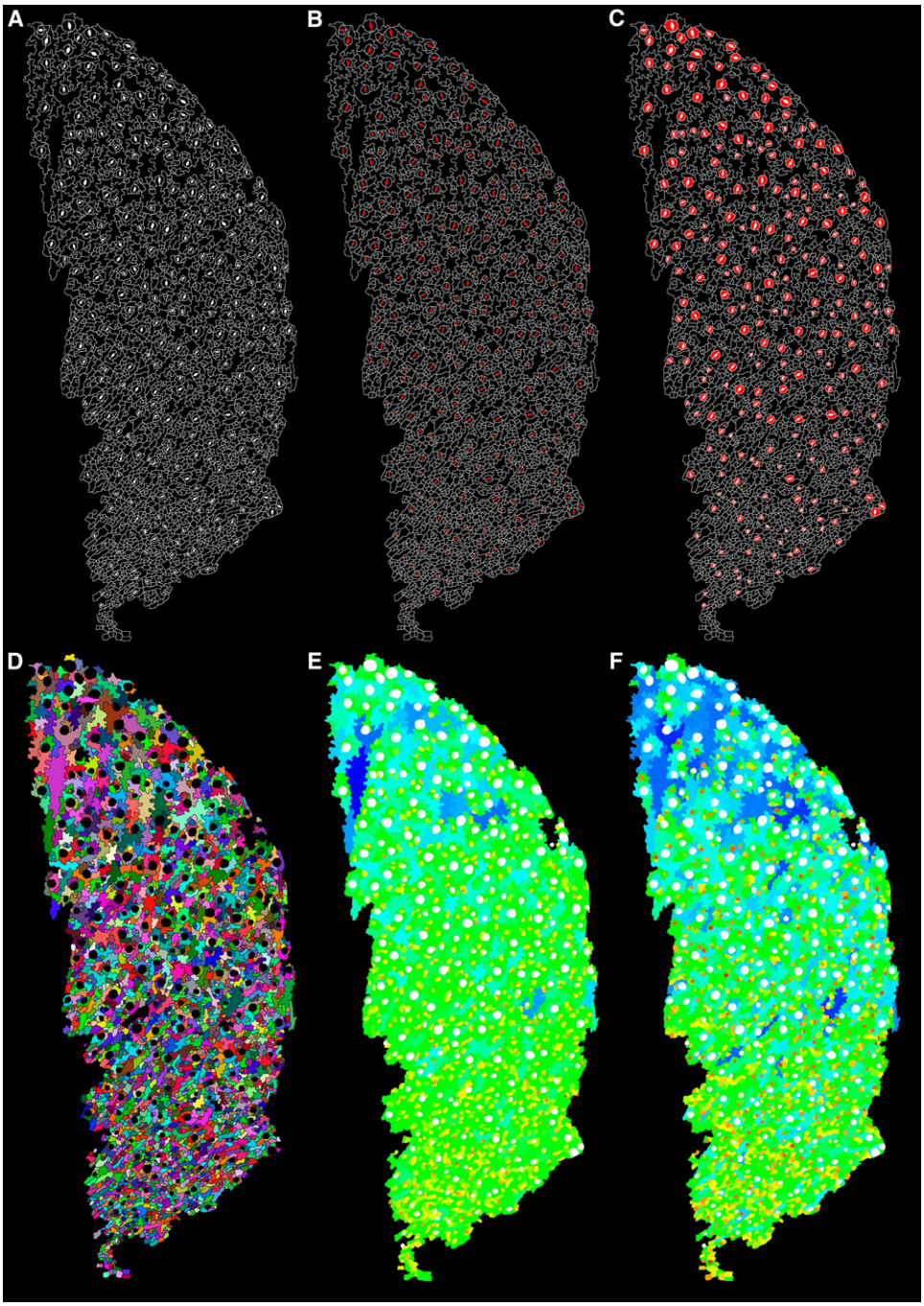

Figure 1. Image Analysis of a Microscopic Drawing of the Abaxial Epidermis of the Third Leaf 12 Days after Stratification

(A) Original microscopic drawing.

(B and C) Guard cells were identified as cells with an area smaller than 500 μm adjacent to the stomatal pores.

(D) Pavement cells randomly colored for visualization of individual cells.

(E) Pavement cells color-coded according to cell size. The color gradient (red-yellow-green-cyan-blue) represents an exponential scale, ranging from the minimum to the maximum cell size measured in the image.

(F) Pavement cells color-coded according to circularity. The color gradient represents a linear scale ranging from the minimum to the maximum cell circularity measured in the image. See also Figure S1 for a representative preprocessed leaf drawing.

Characterization of the Proliferation and Expansion Zones throughout Early Leaf Development

Although the relative length spanned by the proliferation zone in the leaf base decreased throughout development, both the proliferation and expansion zones increased in absolute size as the leaf developed. For the proliferation zone, this growth was achieved primarily through an increase in cell number, because the average cell area remained constant throughout the

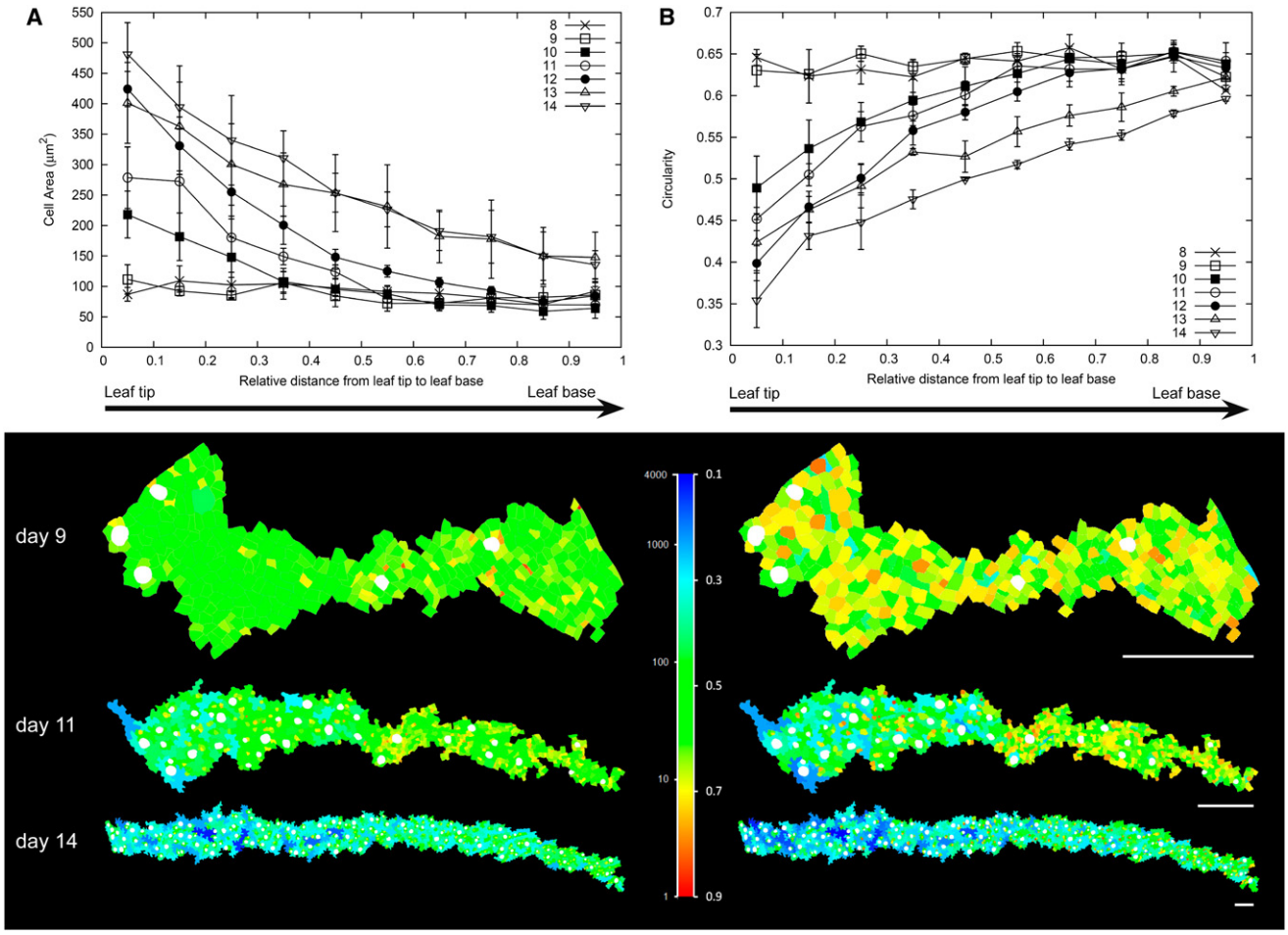

Figure 2. Spatial Distributions of Cell Size and Shape along the Length of the Leaf

The progressive change in cell area and cell shape along the length of the leaf was quantified by calculating the average size and shape of cells within 10-percentile distance bins ranging from the base to the tip of the leaf.

(A) Average cell area in function of the position along the leaf.

(B) Average cell circularity along the leaf. To accommodate for the increasing length of the leaf, position was expressed as the relative distance from the tip to the base and averages were calculated for all cells located in 10% intervals. For both cell area and cell shape, representative images are shown for day 9 (proliferative), day 11 (in transition), and day 14 (expanding) with the tip and base of each leaf aligned with one another to show the relative changes in cell size and shape across leaves at different time points. The color gradient (red-yellow-green-cyan-blue) represents an exponential and linear scale for cell size and circularity, respectively, ranging from the minimum to the maximum measurement in the total time series. Scale bar represents 0.1 mm. Error bars represent the SEM. See also Figure S2 for correlations between cell sizes and shapes.

developmental time series (Figure 3C). For the expansion zone, the cell area increased by 24% between days 10 and 12, whereas its size tripled during the same period (Figure 3C), indicating that the increase in expansion zone size was also primarily due to an increased number of cells shifting from the proliferation to expansion state. Interestingly, the proportion of cells maintained within each zone was highly constant during transition. At all three transition time points (days 10, 11, and 12), approximately 80% of all the cells in the leaf were found in the proliferation zone and approximately 1,000 new cells were recruited each day into the expansion zone to keep a proportion of 20% of the total cells (Figure 3C). Thus, even though the fraction of the leaf made up by the proliferation zone gradually decreased, the absolute size of this zone continued to increase until day 12, after which it abruptly disappeared. The only constant throughout the transition period was the proportion of cells within the two zones.

Stomatal Patterning and Pavement Cell Transition Follow Different Developmental Gradients

Stomatal development during the transition from proliferation to expansion was analyzed in function of position along the leaf by image analysis. To this end, the stomatal index (SI), i.e., the fraction of guard cells in the total population of epidermal cells in a certain region, was calculated throughout the time course on the same images used for the pavement cell measurements. On days 8 and 9, the SI at the tip of leaf 3 was approximately 0.14, indicating that even before any pavement cells had begun to expand, stomatal guard cells had already differentiated in the same area (Figure 4A). At day 10, the SI ranged between 0.1 and

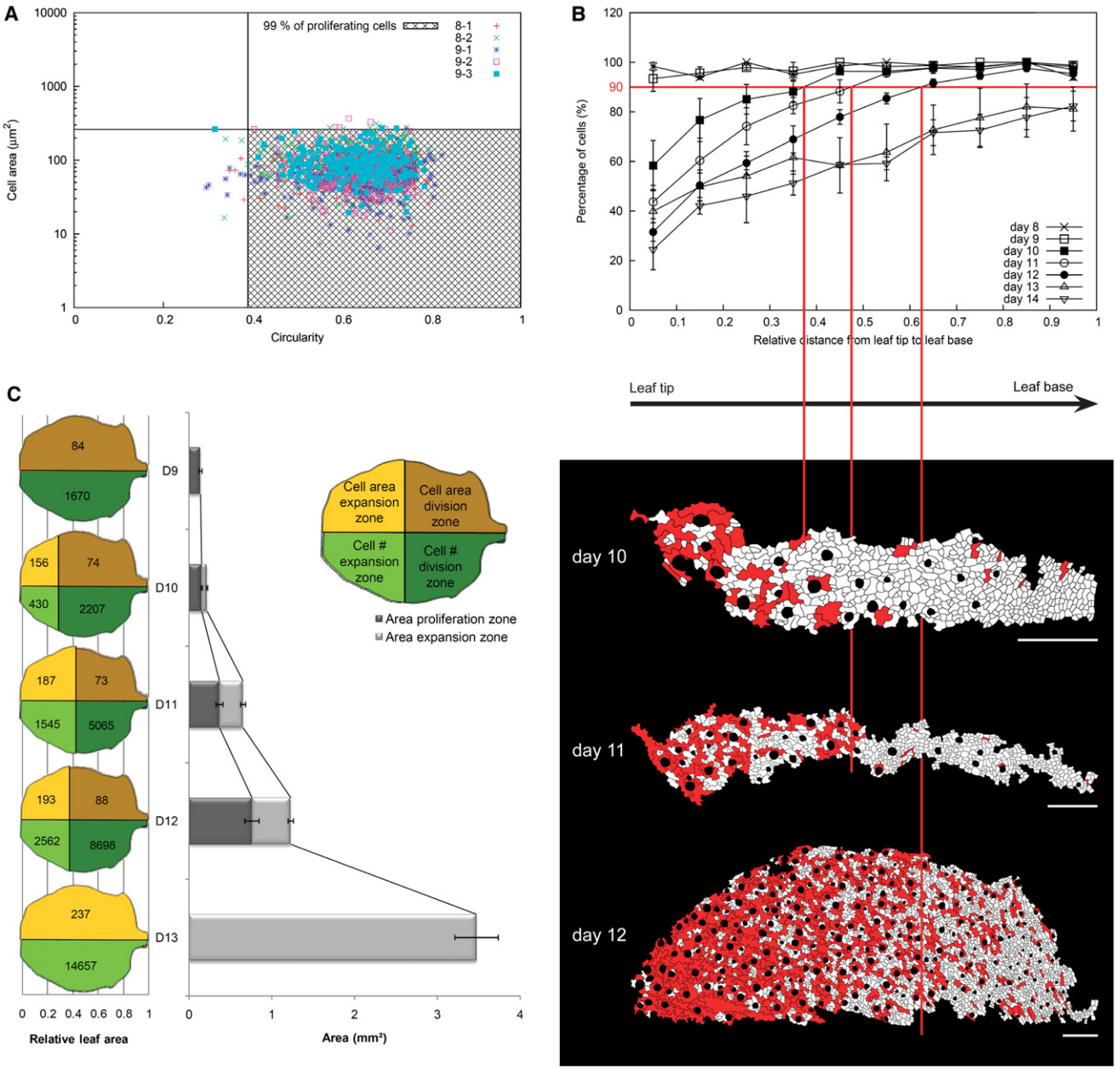

Figure 3. Definition and Characterization of the Proliferation and Expansion Zones

(A) Distribution of cell area and shape measurements of samples at days 8 and 9. Shaded box indicates 99% of the data points used to define the criteria for annotating the proliferation status of the cells for the subsequent time points.

(B) Percentage of cells in each time point that exceeded the proliferation thresholds set in (A) across the relative length of the leaf. Representative images are shown for the three time points during the transition (days 10, 11, and 12). Red-colored cells were defined as expanding according to the cell proliferation criterion established. Red lines mark the boundary region between the expanding and proliferation zones of the leaf.

(C) Relative and absolute areas of the proliferation and expansion zones for time points during the transition. The length of the proliferation arrest front from the leaf base is not to scale. Scale bar represents 0.1 mm. Error bars represent the SEM. See also Figures S3 and S4.

0.25 throughout the entire length of the leaf, excluding only the proximal 15% (Figure 4A), indicating that stomatal differentiation had already occurred even in the highly proliferative zone in the leaf base. Over the subsequent time points, the SI continued to increase throughout the length of the leaf and, at day 14, meristemoids, the stomatal precursor cells, were still present in the tips and bases of the leaves, implying a continued stomatal formation even after the last time point in the analysis (Figure 4B). Moreover, the SI continued to rise even through day 21, once all pavement cells were completely expanded (Skirycz et al., 2010). Nevertheless, at day 14, the leaf tip already showed final values for the SI. These data indicate that stomatal differentiation also

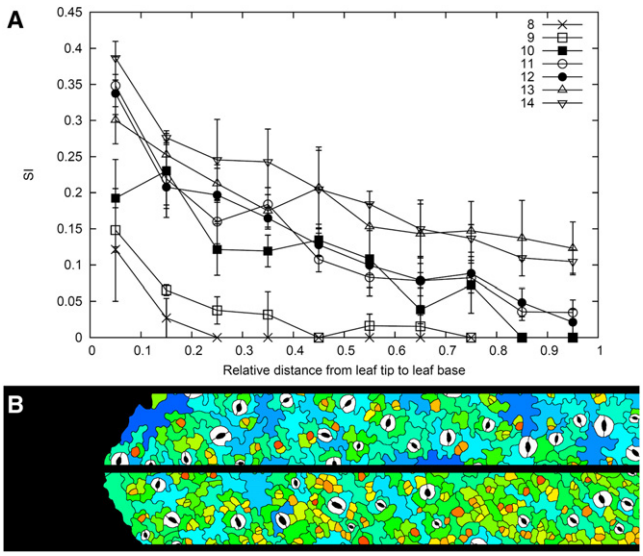

Figure 4. Stomatal Development along the Length of the Leaf
(A) Stomatal index (SI) along the relative length of the leaf.
(B) Image from the distal region (top) and basal region (bottom) of an expanding leaf at day 13. Meristemoids are cells with the highest circularity and are colored red, whereas guard cells are white. Error bars represent the SEM.

follows a temporal and spatial gradient in leaves, but that this gradient is independent from the one driving the transition from pavement cell proliferation to expansion.

Transcriptome Analysis during Transition

To identify the molecular events associated with early leaf development, gene expression profiles from whole leaves at six developmental time points (day 8 to day 13) were analyzed with AGRONOMICS1 tiling arrays (Rehrauer et al., 2010). This genome-wide array probes both the sense and antisense strands, with over 29,920 gene models represented by at least three probes. Over 9,585 genes were differentially regulated between at least two time points, 1,761 of which were not present on the Affymetrix ATH1 microarrays (see Experimental Procedures) (Figure S5A and Table S1). To characterize the gene expression patterns, differentially expressed genes were clustered with a cluster affinity search technique (CAST) (Ben-Dor et al., 1999). A total of 35 clusters were found, with 80% of the genes present in the six main clusters (Figure S6). In general, these six clusters showed gradual expression changes (Figure 5): in the 4,767 genes of clusters 1, 3, and 4, the expression gradually decreased, whereas in the 2,916 genes of clusters 2, 5, and 6, it gradually increased. Functional enrichment, as determined by PageMan (Usadel et al., 2006), revealed that upregulated genes in clusters 2, 5, and 6, were enriched in genes involved in photosynthesis, cell wall synthesis, secondary metabolism, and transport, whereas the downregulated genes in clusters 1, 3, and 4, were enriched for genes involved in general transcription, chromatin remodeling, DNA synthesis, cell cycle, and translation (Figure 5). Of the total number of differentially expressed genes, 18.9% were present only on the tiling array. A similar percentage of tiling array-specific genes were observed within each of these six main clusters. However, the genes that were not clustered, or were in clusters with less than 20 genes, had a much higher proportion, 69% of genes, present only on the tiling array. This observation indicated that the differentially expressed genes present only on the tiling array had distinct expression patterns (Figure S5B). Moreover, as seen previously (Redman et al., 2004; Laubinger et al., 2008; Rehrauer et al., 2010), the expression of many of these genes was low (Figure S5C).

The Sharp Transition from Cell Proliferation to Expansion at Days 10 and 13 Is Supported by the Transcriptome

The morphometric data revealed that cell expansion began abruptly in the tip of leaf 3 at day 10 and in the leaf base at day 13 (Figure 2). To identify more precisely which molecular events coincided with these changes, each pair of consecutive days were compared directly (see Experimental Procedures, Figure 6A, and Figure S7). The majority of transcriptional changes occurred between days 9 and 10, with 2,208 transcripts differentially expressed, of which most were present in clusters 1 and 2. Remarkably, a second wave of transcriptional regulation was observed between days 12 and 13 with 463 transcripts differentially expressed (Figure 6A). Between these abrupt transitional shifts, few transcriptional changes were observed. No more than a total of 210 genes were differentially regulated between days 10 and 12 (Table S1). Genes activated during both transcriptional shifts of differentiation were involved in controlling cell wall formation, primarily the arabinogalactin proteins, fasciclin-like arabinogalactans, expansins, and cellulose synthases, whereas the downregulated genes functioned mostly in cell cycle and cell division (Figures S5B–S5E). Although the same processes were affected at both transitions, the specific genes differed. Genes involved in cell division were enriched at both transitions, but the D-type cyclin gene *CYCD3;2* was the only core cell-cycle gene (Vandepoele et al., 2002) that was repressed during the two transitions and, interestingly, the cell-cycle-inhibitory gene *SIAMESE-RELATED1* (*SMR1*) was the only cell-cycle gene activated over the time course. *SMR1* is highly similar to *SIAMESE* (*SIM*), which has been shown previously to promote endoreduplication (Churchman et al., 2006). This molecular evidence supported the observed morphological transition from cell proliferation to expansion that happens rapidly between days 9 and 10 (onset of cell expansion) and days 12 and 13 (end of cell proliferation) (Figures S5B–S5E), although the precise mechanism probably differs.

Chloroplast Differentiation: An Important Regulator of the Simultaneous Onset of Cell Expansion and Photosynthesis

From the image analysis, we observed that stomata were already visible in the leaf by day 9 (Figure 4) and, correspondingly, between days 8 and 9, carbonic anhydrase transcripts and proteins responsible for shuttling carbon dioxide and regulating stomatal opening and closure were upregulated (Figure S7) (Hu et al., 2010). Thus, this suggests that leaf 3 could start functioning as a photosynthetically active tissue just before the onset of cell expansion. Functional enrichment analysis revealed that indeed, besides cell proliferation and expansion, many processes were affected between days 9 and 10, including

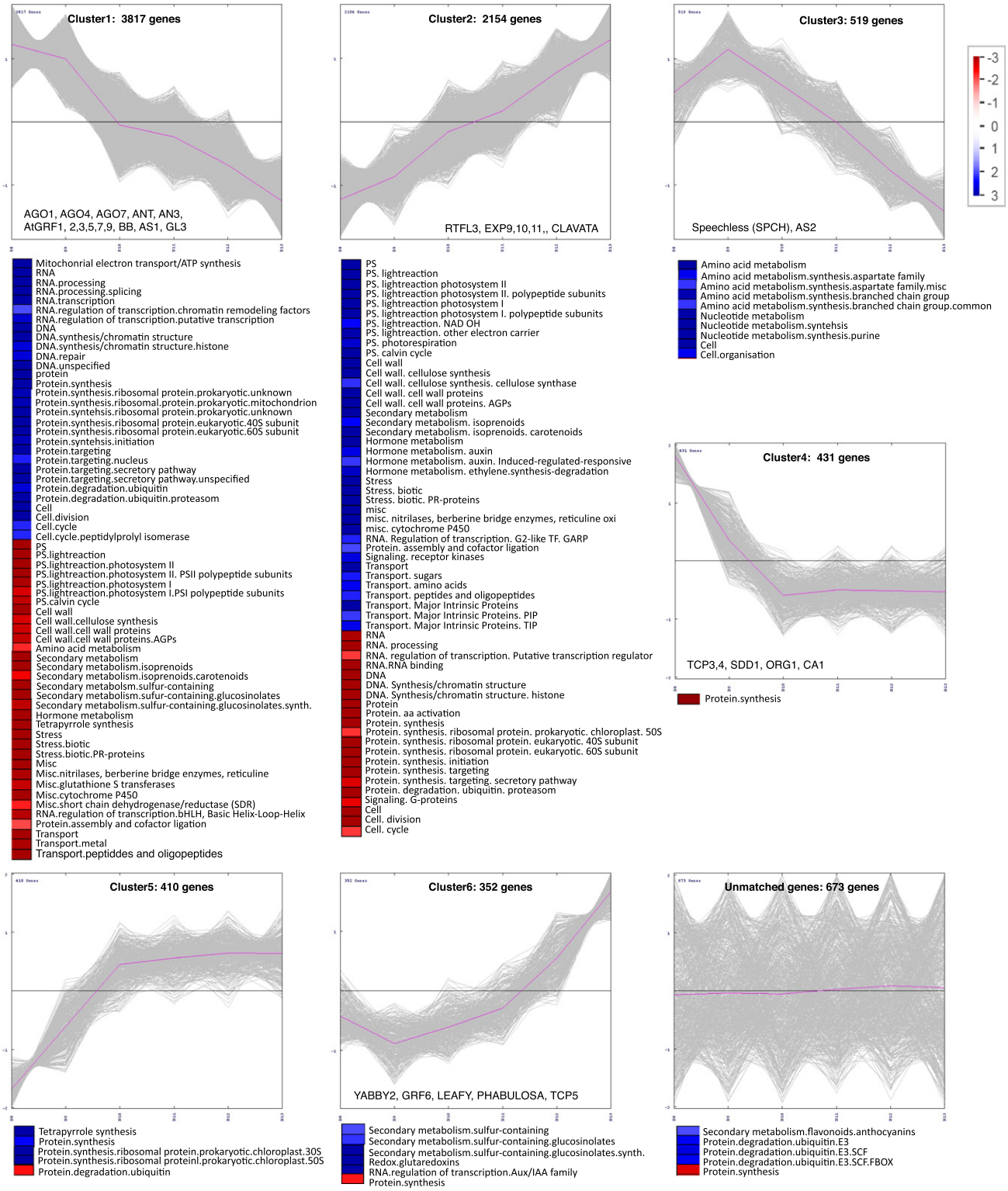

Figure 5. Six Most Populous Clusters and Unclustered Genes from CAST Clustering and PageMan Enrichments of Functional Categories Differentially Expressed within Each Cluster

For clustering, a threshold parameter of 0.759 and a minimum of 20 genes per cluster were used (red, underrepresented; blue, overrepresented). Selected genes previously shown to be involved in leaf development are identified in the cluster they belong. See also Figures S5 and S6 and Table S1 for more details on the transcriptional analysis.

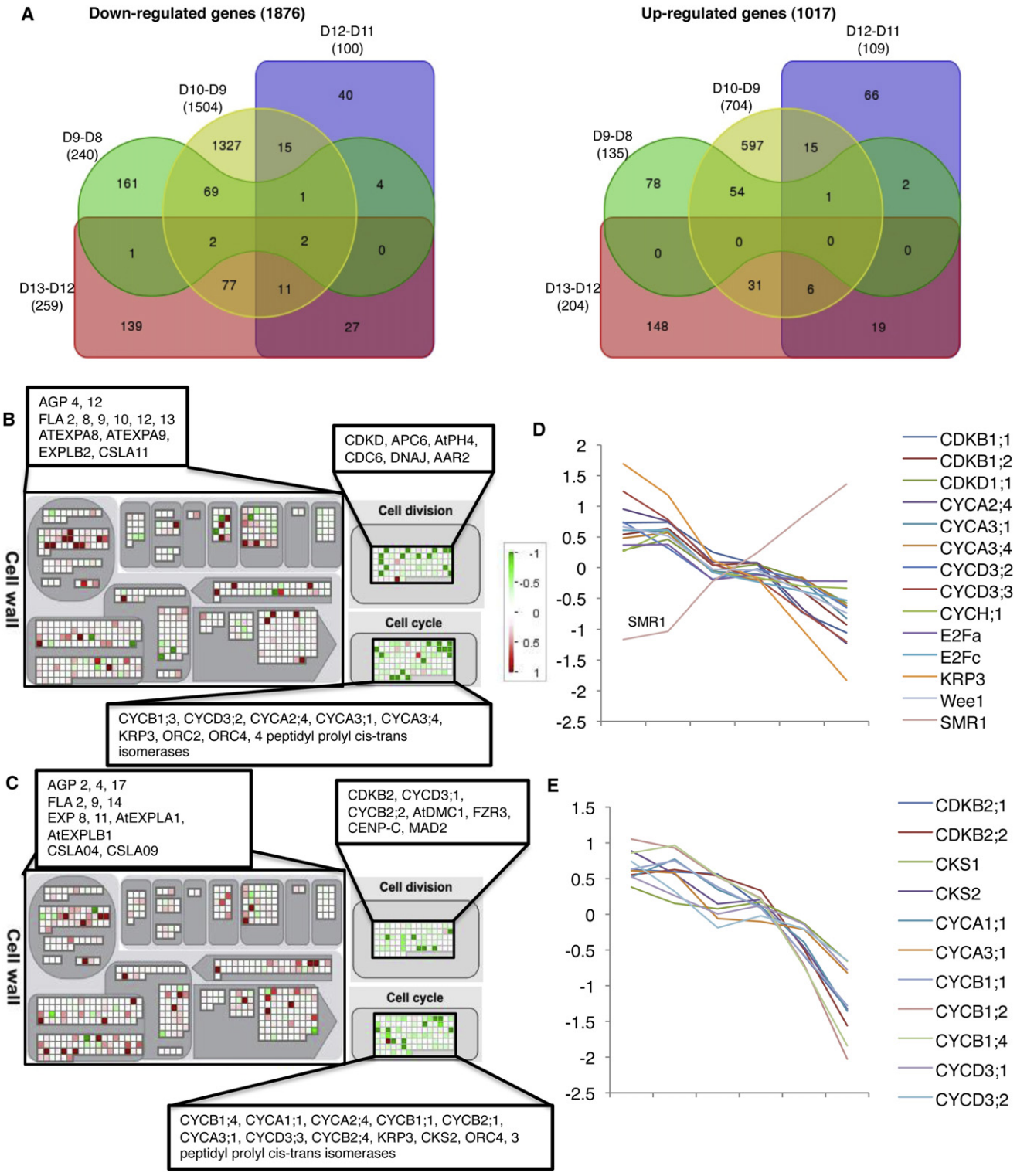

Figure 6. Differentially Expressed Genes between Sequential Time Points

(A) Venn diagram (http://bioinformatics.psb.ugent.be/webtools/Venn/) of total numbers of differentially regulated genes specifically between sequential pairwise comparisons.

(B and C) Selected significantly differentially expressed genes specifically between days 9 and 10 and days 12 and 13, respectively, with FC >0.5 or <−0.5 and p value < 0.05.

(D and E) Expression profiles of core cell-cycle regulators that were significantly differentially expressed (p value < 0.05) between days 9 and 10 and between days 12 and 13, respectively. See also Figure S7.

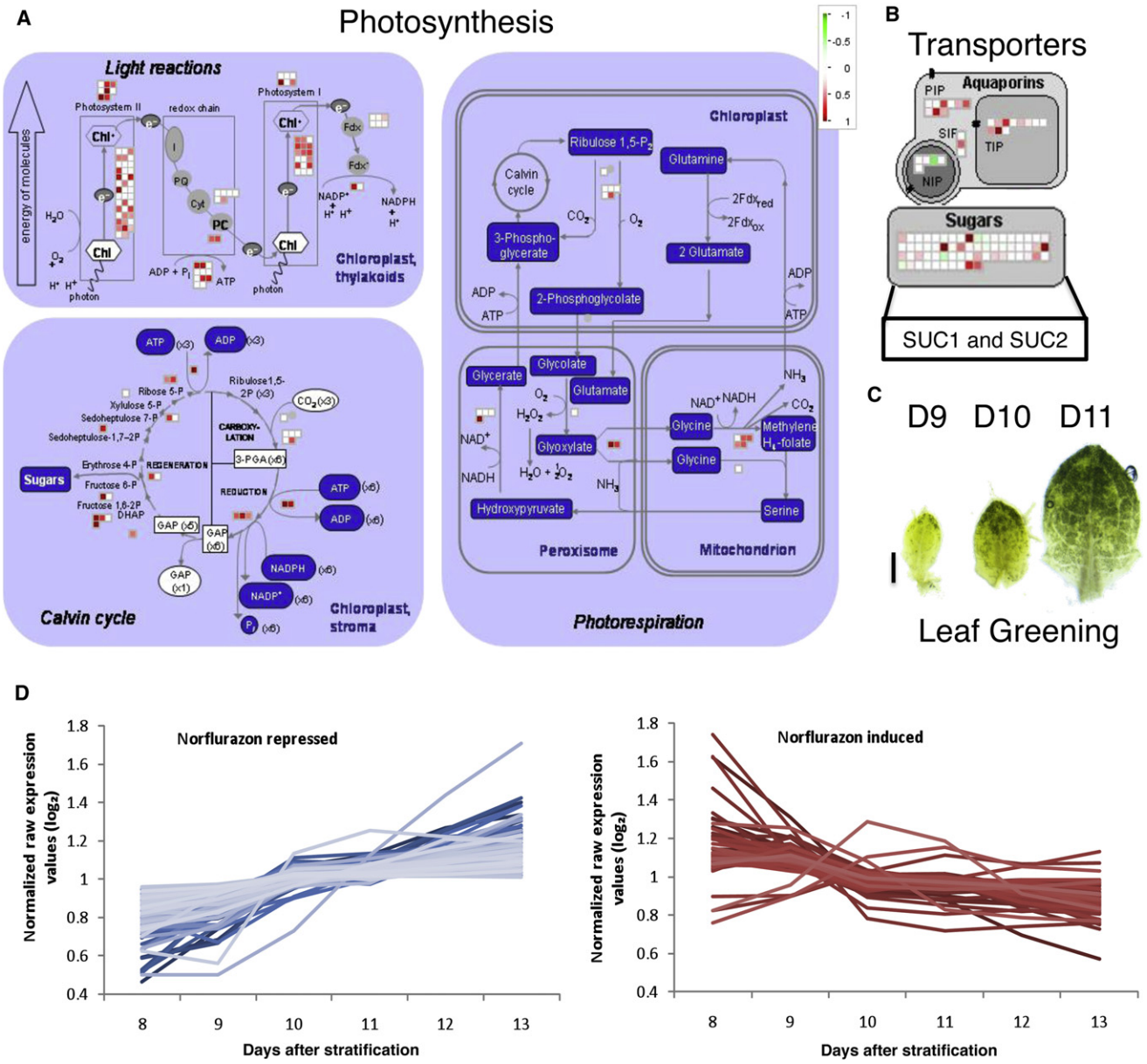

Figure 7. Transcriptional and Morphological Events during Onset of Photomorphogenesis

(A and B) Selected significantly differentially expressed genes specifically between days 9 and 10 with FC >0.5 or <−0.5 involved in photosynthesis and transport, respectively.

(C) Leaf greening shown for days 9, 10, and 11. Scale bar represents 0.25 mm.

(D) Expression profiles for genes differentially expressed in publicly available NF data sets and between days 9 and 10; x axis is days after stratification.

photosynthesis (photosystems I and II, photorespiration, and Calvin cycle) and transport (sugar and water) (Figures 7A and 7B and Figure S7), conspicuously coinciding with the greening of the leaf tip at day 10 that followed a similar basiplastic developmental pattern (Figure 7C). Most interestingly, transcripts in tetrapyrrole synthesis, the biochemical precursors of chlorophylls and hemes, were significantly enriched in cluster 5, which showed increasing expression between days 8 and 9, when the leaf is still fully proliferating (Figure 5). Curiously, the tetrapyrrole pathway was not affected in the branch leading to heme formation; instead, most upregulated genes were upstream of Mg-protoporphyrinogen IX formation, an intermediate in chlorophyll biosynthesis that has been implicated in retrograde signaling (Voigt et al., 2010). These results suggest that chloroplastic retrograde signaling might precede the transition to cell expansion and differentiation of the photosynthetic machinery.

To investigate whether retrograde signaling plays a crucial role in the transition from cell proliferation to expansion, we manipulated this signaling pathway by means of norflurazon (NF), a chemical inhibitor of chloroplast differentiation that had been

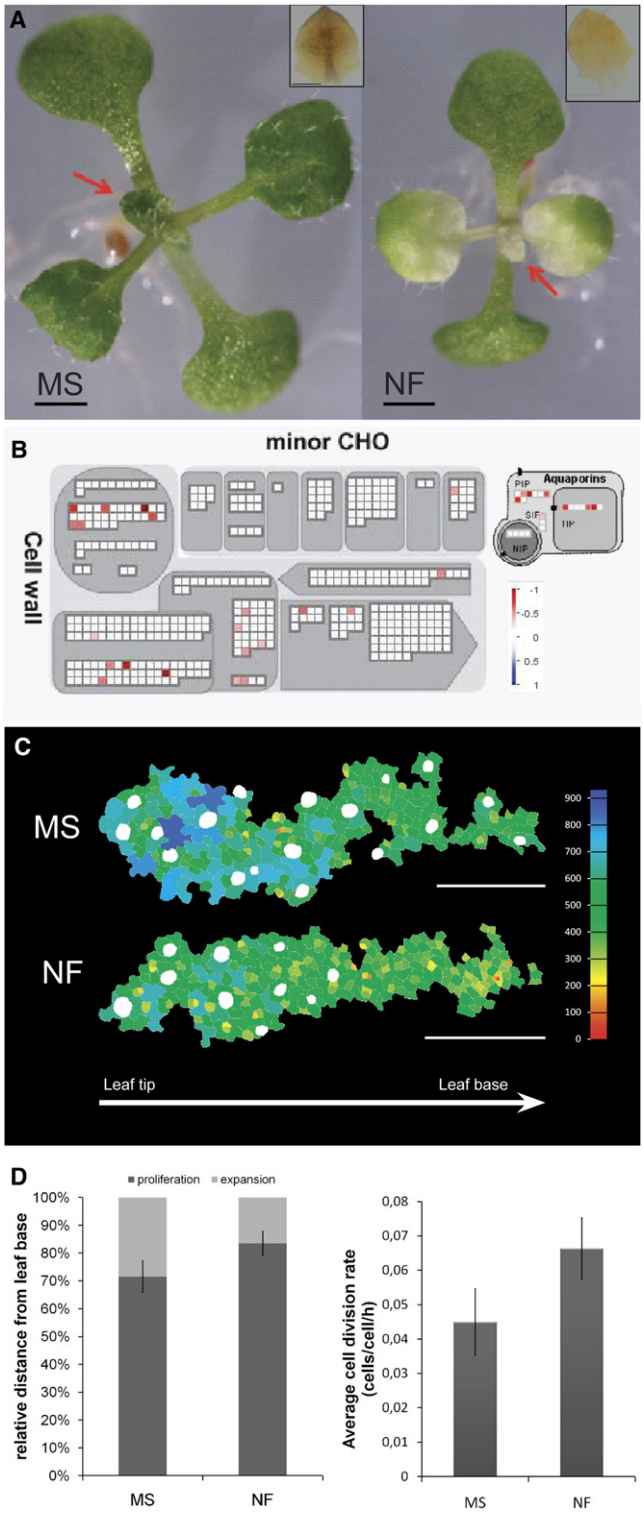

used to detect nuclear genes that might be targeted by retrograde signaling (Koussevitzky et al., 2007). The differentially expressed genes between days 9 and 10 were significantly enriched with genes also found to be differentially expressed in publicly available microarray data sets of plants treated with NF (Strand et al., 2003). In the up- and downregulated genes between days 9 and 10, a 4-fold (p value 9.57×10^{-114}) and 2-fold (p value 1.30×10^{-10}) enrichment was found with genes that were downregulated and upregulated in the publicly available NF data sets, respectively, with most genes showing opposing expression patterns during early leaf development and NF treatment (Figure 7D). To test the specific effects of NF and, thus, chloroplast retrograde signaling on transitioning leaves, plants were analyzed at the transcriptomic and cellular levels after transfer to NF at day 8. Leaf 3 did not develop chloroplasts and, consequently, was blocked in local chloroplast retrograde signaling (Figure 8A). Transcriptional profiling of leaf 3 from these plants revealed that cell wall and water transport proteins were downregulated at day 9, after 1 day of NF treatment (Figure 8B). Simultaneously, markers of chloroplast oxidative stress, such as *CSD2*, were upregulated, indicating that the NF actively affected the sampled tissues and, more specifically, those genes involved in cell expansion and chloroplastic oxidative stress responses. At day 10, photosynthesis was inhibited because transcripts involved in photosystem I and II were downregulated (data not shown) and, in contrast to wild-type leaves, those treated with NF did not accumulate starch (Figure 8A, inset). Cellular analysis revealed that, at day 10, cells of leaves grown on NF were smaller throughout the leaf, even in the proliferation zone, but to a much greater extent in the leaf tip than at the leaf base (data not shown). Similarly, the position of the cell-cycle arrest front in NF-treated samples was closer to the leaf tip (Figure 8C) and leaves grown on NF had a higher cell production rate (Figure 8D) between days 9 and 10 than those grown on Murashige and Skoog (MS) medium, suggesting that the delayed transition is not due to a general inhibition of the developmental processes. These results were confirmed by the CYCB1;1-D-box:GUS-GFP line in which the proliferation zone extended farther along the proximal distal axis in NF-treated than in MS-grown leaves (Figure 8A, inset). To determine whether NF stimulated cell proliferation or inhibited the onset of cell expansion, we transferred plants to NF on day 7 instead of day 8 and harvested leaves 24 hr and 48 hr after transfer. Cellular analysis of these leaves revealed that cell division was unaffected because the cell production was the same in NF-treated and MS-grown leaves, thus indicating that NF did not directly affect cell proliferation, but rather inhibited the onset of cell expansion (Figure 8D). Taken together, these data suggest that retrograde signaling from the chloroplasts is a key factor driving the transition from cell proliferation to cell expansion.

Figure 8. Effects of NF Treatment on the Cell-Cycle Arrest Front

(A) Image of plants at day 11 transferred to NF at day 8. Leaf 3 is indicated by red arrows (note the lack of greening). Scale bar represents 1 mm. Inset is pCYCB1;1::D-box:GUS images and starch staining of leaf 3 at day 10. Scale bar represents 0.25 mm.

(B) MAPMAN representations of enriched genes differentially expressed at day 9 in the third leaves from plants transferred to NF on day 8.

(C) Representative images showing the arrest front position at day 10 for leaf 3 of plants grown on NF and control media (MS). Cells are color-coded based on cell size. Scale bar represents 0.1 mm.

(D) Graphical representations of the relative position of the arrest front from the tip of the leaf and average cell division rate between days 8 and 9 and days 9 and 10 in MS and NF-treated samples. Error bars represent the SEM.

DISCUSSION

The aim of this study was to profile the growth of the leaf at the cellular level by means of image-analysis algorithms and to identify the overall transcriptional responses in young developing leaves to identify how the regulatory networks driving overall leaf development processes are coordinated. The transcriptome profiling allowed us to discern events in the epidermis, such as stomatal formation, and photomorphogenesis in the mesophyll, whereas the epidermal profiling provided the phenotypic characterization of leaf growth at the cellular level. The epidermis was found to be a good marker of cell division status for both the epidermis and mesophyll at these early stages of development. These findings were supported by previous studies that revealed that epidermal cell size correlated well with the mitotic index (Donnelly et al., 1999) and could regulate the overall growth of the leaf (Savaldi-Goldstein et al., 2007; Marcotrigiano, 2010).

Transition to Cell Expansion Is Abrupt

Our current understanding of the transition to secondary morphogenesis is that postmitotic cellular expansion begins in the leaf tip, followed by a cellular differentiation front that moves gradually down the leaf in a basipetal direction (Donnelly et al., 1999; Efroni et al., 2010). From our detailed analyses, it became evident that the transition from primary to secondary morphogenesis was not as gradual as previously thought, despite the gradual expression patterns in the many transcriptional regulators during these time points. No predominant "waves" of transcriptional activity were linked to the differentiation status of the leaf (Efroni et al., 2008), probably because leaf development was followed with high resolution during a short time. Previously, genes of which the expression peaks served as age-specific markers (Efroni et al., 2008) were significantly enriched in the differentially expressed genes of our data set, confirming their developmental importance (data not shown). Taken on a whole-leaf basis, the onset of secondary morphogenesis appeared to progress gradually down the leaf length, but enhanced temporal and spatial resolution revealed two crucial shifts in the transition to secondary morphogenesis in leaf 3.

Possible Mechanisms for Coordinating Cell-Cycle Arrest Front Progression

Although establishment and shutdown of the developmental gradient did not occur gradually, the progression of the arrest front during transition did. Throughout transition, the proliferation zone increased in absolute size, but decreased in the relative length spanned from the leaf base. The relative amount of cells maintained within the proliferation and expansion zones was almost constant across all three time points with 80% ± 4% (SEM) of all cells contained in the proliferation zone. The progression of the cell-cycle arrest front had been hypothesized to be driven by diffusion of a mobile growth factor, inducing cell proliferation and entering the leaf via the petiole (Kazama et al., 2010). One possible candidate, *KLUH* (*KLU*), was identified as regulating such a mobile growth factor and was shown to work in a non-cell-autonomous manner (Anastasiou et al., 2007; Eriksson et al., 2010). However, taking our results into account, it seems more likely that the progression of the cell-cycle arrest front results from a balance between multiple antagonistic processes that act within the expansion and proliferation zones of the transitioning leaf. Such a mechanism might be a consequence of the antagonistic activities of the class I and II *TCP* genes in the control of the expression of cyclin and ribosomal protein genes during cell proliferation (Li et al., 2005), but it is unclear whether they are the main players in the regulation of this gradient.

Coordinated Onset of Cell Expansion and Photosynthesis

As mentioned above, the largest number of transcriptional changes was seen between days 9 and 10 and functional enrichment analysis revealed overrepresentation of genes involved in cell cycle and cell proliferation as well as photosynthesis, carbon sequestration, and sugar and water transporters. Thus, we hypothesized that this time point is critical not only for the establishment of secondary morphogenesis within the leaf, but also for the onset of photosynthesis. Previously, transcripts of the small subunit of ribulose-1,5-bisphosphate-carboxylase had already been detected in less than 100-μm-long leaf primordia of *Amaranthus hypochondriacus* (Ramsperger et al., 1996), but the specific timing of onset of photosynthesis in *Arabidopsis* is still unknown. Imaging revealed that intense greening of the tip of leaf 3 occurred at day 10, overlapping with the region that simultaneously underwent cellular expansion. This observation provides further support that the leaf becomes photosynthetically active at the same time as it shifts from primary to secondary morphogenesis.

Role of Chloroplastic Retrograde Signaling in Regulating Onset of Cell Expansion

Interestingly, a group of genes responsible for tetrapyrrole biosynthesis in chloroplasts were already significantly upregulated prior to most other photosynthetically active enzymes and genes involved in cell expansion, indicating that chloroplast differentiation might initiate before the abrupt transition to cell expansion and photosynthesis. Inhibition of organellar DNA replication is known to repress nuclear DNA replication (Blamire et al., 1974; Rose et al., 1975). To date, the roles of chloroplast retrograde signals coordinating such events are still unclear, although tetrapyrroles, plastid gene expression, reactive oxygen species, and abscisic acid, all are proposed to be involved (Galvez-Valdivieso and Mullineaux, 2010; Voigt et al., 2010). In our data set, only genes that were differentially expressed between days 9 and 10 were strongly enriched with NF-regulated genes (Koussevitzky et al., 2007), providing evidence that retrograde signaling takes place during the abrupt induction of cell expansion and photomorphogenesis. Thus, because chloroplast development preceded that of general photosynthetic maturity and cell expansion, and because retrograde signaling from the chloroplast to the nucleus had been shown to affect nuclear replication and CDKA activity (Kobayashi et al., 2009), chloroplast differentiation was postulated to be a key regulator during early leaf development coordinating and triggering the exit of cell proliferation and subsequent cellular differentiation in the context of both photosynthetic maturity and cell expansion.

In NF-treated leaves, the normal onset of cellular expansion in the leaf tip was strongly inhibited. Two possible situations might explain this phenomenon. First, by blocking retrograde signaling,

cell proliferation was stimulated, thus prolonging the persistence of the cell proliferation zone. This possibility is improbable because retrograde signaling from chloroplasts probably takes place in the leaf tip where the majority of the chloroplasts are differentiated instead of in the leaf base where they are still undifferentiated. Second, by blocking chloroplast retrograde signaling, the onset of cell expansion was inhibited and, coincidentally, cells in the proliferation zone continued to divide until they received a signal to begin expanding. As the size of cells in NF-treated leaves was much more reduced in the tip than those at the base, this possibility seems most plausible and was corroborated by the fact that cell production in NF-treated leaves did not differ from that of MS-grown leaves harvested prior to the onset of transition to cell expansion. Hence, when chloroplast retrograde signaling was blocked, the cell-cycle arrest front was inhibited, primarily due to direct inhibition of cell expansion rather than to prolongation of proliferation. These findings strongly support the idea that proper onset of cell expansion in the leaf tip requires a retrograde signal from the chloroplasts.

Role of Meristemoids in Leaf Growth

Each meristemoid has been shown to divide asymmetrically anywhere from one to three times before giving rise to guard mother cells that will divide symmetrically to form two stomatal guard cells (Peterson et al., 2010). Thus, for every stoma formed, one to three pavement cells arise from its meristemoid precursor. Therefore, the period of meristemoid proliferation is also crucial for determining the final size and shape of the leaf, as corroborated by the development of a dome-shaped enlarged leaf in plants that do not express the genes *PEAPOD1* (*PPD1*) and *PPD2*, which control the arrest of proliferation in meristemoids (White, 2006). In the leaf epidermis, 30% of the cells are guard cells and the remaining 70% are pavement cells, of which 48% are estimated to have arisen from asymmetric divisions of the stomatal lineage (Geisler et al., 2000; Bergmann and Sack, 2007). Thus, meristemoids dictate not only cell patterning, but also regulate the formation of the majority of the pavement cells within the leaf epidermis.

The proliferation program of meristemoids in the epidermis of leaf 3 seemed, intriguingly, independent of the proliferation program of their surrounding pavement cells. Even before any pavement cells had begun expanding, already differentiated stomata were present in the tip of the abaxial leaf epidermis. Moreover, the proliferation of meristemoids also persisted much longer than that of the pavement cells. Already during early leaf development, the SI increased gradually over the proximal-distal axis of the leaf to reach a value in the leaf tip at day 13 that was comparable to the overall SI in the mature leaf (Skirycz et al., 2010). Hence, meristemoid patterning and shutdown of meristemoid proliferation also followed a basipetal gradient, confirming the existence of a previously proposed second cell-cycle arrest front that progressed from tip to base and determined arrest of meristemoid division (White, 2006). However, timing and progression of this secondary arrest front differs substantially from that of the first front that arrests proliferative pavement cell divisions.

In the future, characterization of meristemoid activity with meristemoid marker genes would provide an interesting perspective on how the meristemoid arrest front progresses and, more precisely, how meristemoid divisions contribute to the overall cell number and patterning in the leaf epidermis. Currently, no suitable marker lines can be used in young leaves because most lines have been profiled in highly expanded leaf tissues instead of in fully proliferating tissues and those that have been profiled in leaf primordia do not show meristemoid specificity (Shpak et al., 2005).

In conclusion, we can begin to unravel the role that early leaf development plays in determining the major aspects of leaf morphology, including size, shape, and productivity. From our data, transition from cell proliferation to expansion in pavement cells is clearly not as gradual as commonly assumed and this has strong implications for the regulation of the final leaf size. In fact, the timing of this transition was not only abrupt, but also concurrent with photomorphogenesis. The coregulation of these two transitions may be crucial in understanding how leaves control their cellular differentiation status. Interestingly, by blocking chloroplast-derived retrograde signals, the onset of cell expansion and photomorphogenesis could be inhibited in the leaf tip. In other words, it is crucial for leaves to tightly coordinate the developmental timing of both emergence of cellular expansion and photomorphogenesis, at least in part, by means of a signal from the chloroplasts.

EXPERIMENTAL PROCEDURES

Plant Material and Growth Conditions

Seeds of *A. thaliana* (L.) Heyhn. ecotype Columbia-0 (Col-0) and CYCB1;1-D-box:GUS-GFP (Eloy et al., 2011) were grown on half-strength MS medium (Murashige and Skoog, 1962) and stratified at 4°C for 2 days on plates that were placed in growth rooms kept at 22°C and 16-hr day/8-hr night cycles. Seedlings were harvested at 8, 9, 10, 11, 12, 13, and 14 days after sowing in triplicate. Some of the plants were used for image analysis and others for transcriptome analysis. Tissues for tiling array and image analysis were always harvested at the same time of day, 3 hr after the lights were on. Plants for the NF experiments were grown on permeable nylon meshes on half-strength MS media until day 8, at which time they were transferred to media supplemented with 5 μM NF. Plants were harvested at days 9 and 10 for transcriptomic and cellular analyses.

GUS Staining

CYCB1;1-D-box:GUS plants were infiltrated with heptane for 5 min, left to dry for 5 min, and then were immersed in GUS staining solution as described (Beeckman and Engler, 1994). Plants were vacuum infiltrated for 15 min, subsequently incubated at 37°C for 24 hr, and cleared with 100% ethanol at room temperature for approximately 4 hr. Samples were mounted in lactic acid and imaged under bright-field illumination on a binocular microscope.

Microscopy for Epidermal Cell Size Measurements

Seedlings were cleared in 70% ethanol and the third leaf was removed from the plant and mounted in lactic acid on a microscope slide. The total leaf blade area was measured for 10 representative leaves from each time point under a dark-field binocular microscope. Abaxial epidermal cells along the complete proximal-distal axis of the leaves were drawn with a microscope equipped with differential interference contrast optics (DM LB with 40× and 63× objectives; Leica) and a drawing tube. The entire abaxial epidermis was drawn for samples of representative leaves at days 12 and 13. To image the greening of the leaf, leaf 3 was harvested directly from seedlings at days 9, 10, and 11 with precision microdissection scissors and a binocular microscope. The dissected leaves were mounted in water and imaged directly under a binocular microscope with bright-field illumination.

Image Analysis

The microscopic drawings of the abaxial epidermis were scanned for digitalization. Atypically large cells at the leaf margin and overlaying the midvein were removed with Photoshop (Adobe Systems). Automated preprocessing of the images included: closing small drawing gaps, erasing small extrusions (drawing overshoots), and equally thinning of all the lines. Extraction of stomatal pores allowed the positioning of the stomata within the leaf and the identification of guard cells (cells <500 μm neighboring the stomatal pores). The remaining nonguard cells were identified as pavement cells and were used for morphological analysis. For each pavement cell, we determined the center of mass, the cell size, and circularity [4π*(area/perimeter)]. All data were calibrated according to the microscopic enlargement used to produce the drawings. The cells were color-coded according to their size and circularity, along an exponential and linear scale, respectively. The color gradient (red-yellow-green-cyan-blue) ranged from the minimum to the maximum size/circularity measured within the image or within the complete set of figures. The image analysis algorithms were written in C++ scripting, making use of the SDC Morphology Toolbox for C++ (http://www.mmorph.com/cppmorph/) and the ImageJ macro language (http://rsbweb.nih.gov/ij/). All data were analyzed by scripts written in Perl programming language (http://www.perl.org/) and graphs were plotted with Gnuplot (http://www.gnuplot.info/). Image and data analysis scripts are available upon request.

Material for Transcriptomic Analysis

Seedlings for transcriptomic analysis were placed in RNAlater (Ambion) and stored at 4°C until leaf 3 could be dissected from the plant. Plants stayed in RNAlater no longer than 5 days and dissected on a cooling plate under a stereomicroscope with precision microdissection scissors. The excised leaves were deposited in a new tube, frozen, and ground with a 3-mm metal ball (Retsch MM301). A minimum and maximum of 64 (day 13) and 256 (day 8) leaves per replicate were harvested.

RNA Extraction

RNA was extracted from the samples, each replicate independently, with the RNeasy mini kit (QIAGEN) and on-column DNase digestion by means of the Qiacube (QIAGEN) robot.

AGRONOMICS1 Tiling Array Hybridizations and Data Analysis

RNA samples were prepared at the Eidgenössische Technische Hochschule (ETH; Zürich, Switzerland) with the microarray target preparation method 3 and hybridized as described (Rehrauer et al., 2010). Expression data were processed with Robust Multichip Average (RMA; background correction, normalization, and summarization) as implemented in BioConductor (Irizarry et al., 2003; Gentleman et al., 2004). Dynamic probe selection was performed, only keeping probes that changed in expression over the six time points (Rehrauer et al., 2010). The BioConductor package Limma was used to identify differentially expressed genes (Smyth, 2004). Genes that were differentially expressed between at least two time points were identified with a moderated F-test and a corrected p value of 0.05. Pairwise comparisons between time points were tested with moderated *t* statistics and eBayes method as implemented in Limma. p values were corrected for multiple testing (for each contrast separately with topTable; Hochberg and Benjamini, 1990). The differentially expressed genes were CAST clustered with TMEV, a threshold parameter of 0.759, and a limit of minimum 20 genes per cluster. Transcription factors were identified by their annotation in the Gene Ontology (GO) and the *Arabidopsis* Gene Regulatory Information Server (AGRIS) databases (Davuluri et al., 2003; Harris et al., 2004). Differentially expressed genes were compared to gene expression data from publicly available microarrays downloaded from the Gene Expression Omnibus (GEO) (Edgar et al., 2002). Significant overlaps between these data sets were identified by means of Fisher's exact tests, followed by Bonferroni p value correction. Functional enrichments were calculated with PageMan (Usadel et al., 2006) and visualized with MAPMAN (Thimm et al., 2004).

ACCESSION NUMBERS

Microarray data have been deposited in the NCBI Gene Expression Omnibus, and the GEO series accession number is GSE33936.

SUPPLEMENTAL INFORMATION

Supplemental Information includes seven figures and one table and can be found with this article online at doi:10.1016/j.devcel.2011.11.011.

ACKNOWLEDGMENTS

We thank all colleagues of the Systems Biology of Yield research group for fruitful discussions and Martine De Cock for help in preparing the manuscript. This work was supported by grants from the Belgian Network BARN (Growth and Development of Higher Plants IUAP VI/33), funded by the Interuniversity Attraction Poles Program, initiated by the Belgian State, Science Policy Office, the "Bijzonder Onderzoeksfonds Methusalem Project" (BOF08/01M00408) of the Ghent University, the European Community Grant FP6 IP AGRON-OMICS (LSHG-CT-2006-037704). S.D. is indebted to the Agency for Innovation through Science and Technology for a predoctoral fellowship. S.D.B. is a postdoctoral fellow and F.C. was a research fellow of the Research Foundation-Flanders. P.M. is the recipient of a Marie Curie Intra-European Fellowships for Career Development (PIEF-GA-2009-235827).

Received: October 8, 2010
Revised: September 8, 2011
Accepted: November 23, 2011
Published online: January 5, 2012

REFERENCES

Anastasiou, E., Kenz, S., Gerstung, M., MacLean, D., Timmer, J., Fleck, C., and Lenhard, M. (2007). Control of plant organ size by *KLUH/CYP78A5*-dependent intercellular signaling. Dev. Cell *13*, 843–856.

Beeckman, T., and Engler, G. (1994). An easy technique for the clearing of histochemically stained plant tissue. Plant Mol. Biol. Rep. *12*, 37–42.

Beemster, G.T.S., and Baskin, T.I. (1998). Analysis of cell division and elongation underlying the developmental acceleration of root growth in *Arabidopsis thaliana*. Plant Physiol. *116*, 1515–1526.

Beemster, G.T.S., Fiorani, F., and Inzé, D. (2003). Cell cycle: the key to plant growth control? Trends Plant Sci. *8*, 154–158.

Beemster, G.T.S., De Veylder, L., Vercruysse, S., West, G., Rombaut, D., Van Hummelen, P., Galichet, A., Gruissem, W., Inzé, D., and Vuylsteke, M. (2005). Genome-wide analysis of gene expression profiles associated with cell cycle transitions in growing organs of Arabidopsis. Plant Physiol. *138*, 734–743.

Ben-Dor, A., Shamir, R., and Yakhini, Z. (1999). Clustering gene expression patterns. J. Comput. Biol. *6*, 281–297.

Bergmann, D.C., and Sack, F.D. (2007). Stomatal development. Annu. Rev. Plant Biol. *58*, 163–181.

Berná, G., Robles, P., and Micol, J.L. (1999). A mutational analysis of leaf morphogenesis in *Arabidopsis thaliana*. Genetics *152*, 729–742.

Blamire, J., Flechtner, V.R., and Sager, R. (1974). Regulation of nuclear DNA replication by thechloroplast in *Chlamydomonas*. Proc. Natl. Acad. Sci. USA *71*, 2867–2871.

Boudolf, V., Lammens, T., Boruc, J., Van Leene, J., Van Den Daele, H., Maes, S., Van Isterdael, G., Russinova, E., Kondorosi, E., Witters, E., et al. (2009). CDKB1;1 forms a functional complex with CYCA2;3 to suppress endocycle onset. Plant Physiol. *150*, 1482–1493.

Braybrook, S.A., and Kuhlemeier, C. (2010). How a plant builds leaves. Plant Cell *22*, 1006–1018.

Byrne, M.E. (2005). Networks in leaf development. Curr. Opin. Plant Biol. *8*, 59–66.

Churchman, M.L., Brown, M.L., Kato, N., Kirik, V., Hülskamp, M., Inzé, D., De Veylder, L., Walker, J.D., Zheng, Z., Oppenheimer, D.G., et al. (2006). SIAMESE, a plant-specific cell cycle regulator, controls endoreplication onset in *Arabidopsis thaliana*. Plant Cell *18*, 3145–3157.

Cosgrove, D.J. (2005). Growth of the plant cell wall. Nat. Rev. Mol. Cell Biol. *6*, 850–861.

Davuluri, R.V., Sun, H., Palaniswamy, S.K., Matthews, N., Molina, C., Kurtz, M., and Grotewold, E. (2003). AGRIS: Arabidopsis Gene Regulatory Information Server, an information resource of Arabidopsis cis-regulatory elements and transcription factors. BMC Bioinformatics *4*, 25.1–25.11.

de Reuille, P.B., Bohn-Courseau, I., Ljung, K., Morin, H., Carraro, N., Godin, C., and Traas, J. (2006). Computer simulations reveal properties of the cell-cell signaling network at the shoot apex in *Arabidopsis*. Proc. Natl. Acad. Sci. USA *103*, 1627–1632.

De Veylder, L., Beeckman, T., Beemster, G.T.S., Krols, L., Terras, F., Landrieu, I., van der Schueren, E., Maes, S., Naudts, M., and Inzé, D. (2001). Functional analysis of cyclin-dependent kinase inhibitors of Arabidopsis. Plant Cell *13*, 1653–1668.

Dhondt, S., Coppens, F., De Winter, F., Swarup, K., Merks, R.M.H., Inzé, D., Bennett, M.J., and Beemster, G.T.S. (2010). SHORT-ROOT and SCARECROW regulate leaf growth in Arabidopsis by stimulating S-phase progression of the cell cycle. Plant Physiol. *154*, 1183–1195.

Donnelly, P.M., Bonetta, D., Tsukaya, H., Dengler, R.E., and Dengler, N.G. (1999). Cell cycling and cell enlargement in developing leaves of *Arabidopsis*. Dev. Biol. *215*, 407–419.

Edgar, R., Domrachev, M., and Lash, A.E. (2002). Gene Expression Omnibus: NCBI gene expression and hybridization array data repository. Nucleic Acids Res. *30*, 207–210.

Efroni, I., Blum, E., Goldshmidt, A., and Eshed, Y. (2008). A protracted and dynamic maturation schedule underlies *Arabidopsis* leaf development. Plant Cell *20*, 2293–2306.

Efroni, I., Eshed, Y., and Lifschitz, E. (2010). Morphogenesis of simple and compound leaves: a critical review. Plant Cell *22*, 1019–1032.

Eloy, N.B., de Freitas Lima, M., Van Damme, D., Vanhaeren, H., Gonzalez, N., De Milde, L., Hemerly, A.S., Beemster, G.T.S., Inzé, D., and Ferreira, P.C.G. (2011). The APC/C subunit 10 plays an essential role in cell proliferation during leaf development. Plant J. *68*, 351–363.

Eriksson, S., Stransfeld, L., Adamski, N.M., Breuninger, H., and Lenhard, M. (2010). *KLUH/CYP78A5*-dependent growth signaling coordinates floral organ growth in *Arabidopsis*. Curr. Biol. *20*, 527–532.

Galvez-Valdivieso, G., and Mullineaux, P.M. (2010). The role of reactive oxygen species in signalling from chloroplasts to the nucleus. Physiol. Plant. *138*, 430–439.

Geisler, M., Nadeau, J., and Sack, F.D. (2000). Oriented asymmetric divisions that generate the stomatal spacing pattern in arabidopsis are disrupted by the *too many mouths* mutation. Plant Cell *12*, 2075–2086.

Gentleman, R.C., Carey, V.J., Bates, D.M., Bolstad, B., Dettling, M., Dudoit, S., Ellis, B., Gautier, L., Ge, Y., Gentry, J., et al. (2004). Bioconductor: open software development for computational biology and bioinformatics. Genome Biol. *5*, R80.1–R80.16.

Gonzalez, N., Beemster, G.T.S., and Inzé, D. (2009). David and Goliath: what can the tiny weed *Arabidopsis* teach us to improve biomass production in crops? Curr. Opin. Plant Biol. *12*, 157–164.

Gonzalez, N., De Bodt, S., Sulpice, R., Jikumaru, Y., Chae, E., Dhondt, S., Van Daele, T., De Milde, L., Weigel, D., Kamiya, Y., et al. (2010). Increased leaf size: different means to an end. Plant Physiol. *153*, 1261–1279.

Green, P.B. (1976). Growth and cell pattern formation on an axis: critique of concepts, terminology, and modes of study. Bot. Gaz. *137*, 187–202.

Harris, M.A., Clark, J., Ireland, A., Lomax, J., Ashburner, M., Foulger, R., Eilbeck, K., Lewis, S., Marshall, B., Mungall, C., et al; Gene Ontology Consortium. (2004). The Gene Ontology (GO) database and informatics resource. Nucleic Acids Res. *32* (Database issue), D258–D261.

Hochberg, Y., and Benjamini, Y. (1990). More powerful procedures for multiple significance testing. Stat. Med. *9*, 811–818.

Horiguchi, G., Fujikura, U., Ferjani, A., Ishikawa, N., and Tsukaya, H. (2006). Large-scale histological analysis of leaf mutants using two simple leaf observation methods: identification of novel genetic pathways governing the size and shape of leaves. Plant J. *48*, 638–644.

Horiguchi, G., Gonzalez, N., Beemster, G.T.S., Inzé, D., and Tsukaya, H. (2009). Impact of segmental chromosomal duplications on leaf size in the *grandifolia-D* mutants of *Arabidopsis thaliana*. Plant J. *60*, 122–133.

Hu, H., Boisson-Dernier, A., Israelsson-Nordström, M., Böhmer, M., Xue, S., Ries, A., Godoski, J., Kuhn, J.M., and Schroeder, J.I. (2010). Carbonic anhydrases are upstream regulators of CO_2-controlled stomatal movements in guard cells. Nat. Cell Biol. *12*, 87–93, 1–18.

Irizarry, R.A., Hobbs, B., Collin, F., Beazer-Barclay, Y.D., Antonellis, K.J., Scherf, U., and Speed, T.P. (2003). Exploration, normalization, and summaries of high density oligonucleotide array probe level data. Biostatistics *4*, 249–264.

Kazama, T., Ichihashi, Y., Murata, S., and Tsukaya, H. (2010). The mechanism of cell cycle arrest front progression explained by a *KLUH/CYP78A5*-dependent mobile growth factor in developing leaves of *Arabidopsis thaliana*. Plant Cell Physiol. *51*, 1046–1054.

Kobayashi, Y., Kanesaki, Y., Tanaka, A., Kuroiwa, H., Kuroiwa, T., and Tanaka, K. (2009). Tetrapyrrole signal as a cell-cycle coordinator from organelle to nuclear DNA replication in plant cells. Proc. Natl. Acad. Sci. USA *106*, 803–807.

Koussevitzky, S., Nott, A., Mockler, T.C., Hong, F., Sachetto-Martins, G., Surpin, M., Lim, J., Mittler, R., and Chory, J. (2007). Signals from chloroplasts converge to regulate nuclear gene expression. Science *316*, 715–719.

Laubinger, S., Zeller, G., Henz, S.R., Sachsenberg, T., Widmer, C.K., Naouar, N., Vuylsteke, M., Schölkofp, B., Rätsch, G., and Weigel, D. (2008). At-TAX: a whole genome tiling array resource for developmental expression analysis and transcript identification in *Arabidopsis thaliana*. Genome Biol. *9*, R112.1–R112.16.

Lee, Y.K., Kim, G.-T., Kim, I.-J., Park, J., Kwak, S.-S., Choi, G., and Chung, W.-I. (2006). *LONGIFOLIA1* and *LONGIFOLIA2*, two homologous genes, regulate longitudinal cell elongation in *Arabidopsis*. Development *133*, 4305–4314.

Li, C., Potuschak, T., Colón-Carmona, A., Gutiérrez, R.A., and Doerner, P. (2005). *Arabidopsis* TCP20 links regulation of growth and cell division control pathways. Proc. Natl. Acad. Sci. USA *102*, 12978–12983.

Li, Y., Zheng, L., Corke, F., Smith, C., and Bevan, M.W. (2008). Control of final seed and organ size by the *DA1* gene family in *Arabidopsis thaliana*. Genes Dev. *22*, 1331–1336.

Marcotrigiano, M. (2010). A role for leaf epidermis in the control of leaf size and the rate and extent of mesophyll cell division. Am. J. Bot. *97*, 224–233.

Mizukami, Y., and Fischer, R.L. (2000). Plant organ size control: AINTEGUMENTA regulates growth and cell numbers during organogenesis. Proc. Natl. Acad. Sci. USA *97*, 942–947.

Murashige, T., and Skoog, F. (1962). A revised medium for rapid growth and bio assays with tobacco tissue cultures. Physiol. Plant. *15*, 473–497.

Pérez-Pérez, J.M., Candela, H., Robles, P., Quesada, V., Ponce, M.R., and Micol, J.L. (2009). Lessons from a search for leaf mutants in *Arabidopsis thaliana*. Int. J. Dev. Biol. *53*, 1623–1634.

Pesch, M., and Hülskamp, M. (2009). One, two, three…models for trichome patterning in *Arabidopsis?* Curr. Opin. Plant Biol. *12*, 587–592.

Peterson, K.M., Rychel, A.L., and Torii, K.U. (2010). Out of the mouths of plants: the molecular basis of the evolution and diversity of stomatal development. Plant Cell *22*, 296–306.

Ramsperger, V.C., Summers, R.G., and Berry, J.O. (1996). Photosynthetic gene expression in meristems and during initial leaf development in a C_4 dicotyledonous plant. Plant Physiol. *111*, 999–1010.

Redman, J.C., Haas, B.J., Tanimoto, G., and Town, C.D. (2004). Development and evaluation of an *Arabidopsis* whole genome Affymetrix probe array. Plant J. *38*, 545–561.

Rehrauer, H., Aquino, C., Gruissem, W., Henz, S.R., Hilson, P., Laubinger, S., Naouar, N., Patrignani, A., Rombauts, S., Shu, H., et al. (2010). AGRONOMICS1: a new resource for Arabidopsis transcriptome profiling. Plant Physiol. *152*, 487–499.

Rose, R.J., Cran, D.G., and Possingham, J.V. (1975). Changes in DNA synthesis during cell growth and chloroplast replication in greening spinach leaf disks. J. Cell Sci. *17*, 27–41.

Savaldi-Goldstein, S., Peto, C., and Chory, J. (2007). The epidermis both drives and restricts plant shoot growth. Nature *446*, 199–202.

Scarpella, E., Barkoulas, M., and Tsiantis, M. (2010). Control of leaf and vein development by auxin. Cold Spring Harb Perspect Biol *2*, a001511.

Shpak, E.D., McAbee, J.M., Pillitteri, L.J., and Torii, K.U. (2005). Stomatal patterning and differentiation by synergistic interactions of receptor kinases. Science *309*, 290–293.

Skirycz, A., De Bodt, S., Obata, T., De Clercq, I., Claeys, H., De Rycke, R., Andriankaja, M., Van Aken, O., Van Breusegem, F., Fernie, A.R., and Inzé, D. (2010). Developmental stage specificity and the role of mitochondrial metabolism in the response of Arabidopsis leaves to prolonged mild osmotic stress. Plant Physiol. *152*, 226–244.

Smyth, G.K. (2004). Linear models and empirical Bayes methods for assessing differential expression in microarray experiments. Stat. Appl. Genet. Mol. Biol. *3*, Article 3.

Strand, Å., Asami, T., Alonso, J., Ecker, J.R., and Chory, J. (2003). Chloroplast to nucleus communication triggered by accumulation of Mg-protoporphyrinIX. Nature *421*, 79–83.

Thimm, O., Bläsing, O., Gibon, Y., Nagel, A., Meyer, S., Krüger, P., Selbig, J., Müller, L.A., Rhee, S.Y., and Stitt, M. (2004). MAPMAN: a user-driven tool to display genomics data sets onto diagrams of metabolic pathways and other biological processes. Plant J. *37*, 914–939.

Traas, J., and Monéger, F. (2010). Systems biology of organ initiation at the shoot apex. Plant Physiol. *152*, 420–427.

Tsukaya, H. (2002). Interpretation of mutants in leaf morphology: genetic evidence for a compensatory system in leaf morphogenesis that provides a new link between cell and organismal theories. Int. Rev. Cytol. *217*, 1–39.

Tsukaya, H. (2003). Organ shape and size: a lesson from studies of leaf morphogenesis. Curr. Opin. Plant Biol. *6*, 57–62.

Usadel, B., Nagel, A., Steinhauser, D., Gibon, Y., Bläsing, O.E., Redestig, H., Sreenivasulu, N., Krall, L., Hannah, M.A., Poree, F., Fernie, A.R., and Stitt, M. (2006). PageMan: an interactive ontology tool to generate, display, and annotate overview graphs for profiling experiments. BMC Bioinformatics *7*, 535.1–535.8.

Vandepoele, K., Raes, J., De Veylder, L., Rouzé, P., Rombauts, S., and Inzé, D. (2002). Genome-wide analysis of core cell cycle genes in Arabidopsis. Plant Cell *14*, 903–916.

Voigt, C., Oster, U., Börnke, F., Jahns, P., Dietz, K.-J., Leister, D., and Kleine, T. (2010). In-depth analysis of the distinctive effects of norflurazon implies that tetrapyrrole biosynthesis, organellar gene expression and ABA cooperate in the GUN-type of plastid signalling. Physiol. Plant. *138*, 503–519.

White, D.W.R. (2006). *PEAPOD* regulates lamina size and curvature in *Arabidopsis*. Proc. Natl. Acad. Sci. USA *103*, 13238–13243.